Progress In Electromagnetics Research C, Vol. 78, 69–81, 2017

Design and Development of a Multi-Feed End-Fired Microstrip Antenna for TCAS Airborne System

Debajit De* **and Prasanna K. Sahu**

Abstract—Traffic alert and Collision Avoidance System (TCAS) is an airborne system which is designed to provide the service as a last defense equipment for avoiding mid-air collisions between the aircraft. In such airborne systems, where low aerodynamic drag is urgently required, the end-fire antenna is suitable to be used. An effort to develop such an antenna, using microstrip elements, is described in this paper. Here, a Multi-Feed Microstrip Antenna is presented which radiates in the end-fire direction. The proposed antenna is designed in such a way that it can radiate the whole 360° surveillance region of the aircraft. To encapsulate the antenna inside an enclosure, an aerodynamically shaped Radome is also designed and presented in this paper. For designing this antenna model and its Radome, CST Microwave Studio is used here as the EM tool. The performance and other antenna characteristics have been explored from the simulation results followed by the antenna fabrication and measurement. Quite good agreement is achieved between the simulated and measured results. Much better performance characteristics make this proposed antenna a good candidate for this application.

1. INTRODUCTION

Traffic Alert and Collision Avoidance System (TCAS) provides a solution to reduce the risk of mid-air collisions between aircraft. TCAS is an airborne system which is independent from the ground based Air Traffic Control (ATC) unit, and it protects the aircraft from the mid-air collisions. TCAS makes use of the radar beacon transponders carried by an aircraft for ground ATC purposes and provides no protection against aircraft which do not have an operating transponder [1]. Federal Aviation Administration (FAA), Civil Aviation Authorities (CAA) and other aviation agencies have extensively analyzed the flight evaluation systems throughout many years. As a consequence, those governing bodies proposed the TCAS to minimize the collisions between aircraft in mid-air [2].

For surveillance of any surrounding aircraft, TCAS sends interrogation with a consistent rate, ostensibly once in every second and utilizes a recipient for distinguishing the responds to these transmitting signals which are coming from all the transponders of close-by aircraft as shown in Figure 1. An overall block diagram of the TCAS system is presented in Figure 2.

TCAS consists of a Mode S/TCAS Control Panel, a Mode S Transponder, a TCAS Computer, Antennas, Traffic and Resolution Advisory Displays and an Aural Annunciator [3]. The conventional top mounted directional antenna in present TCAS system is shown in Figure 3(a). It consists of an array with four steerable and passive radiating stubs, which are oriented at 0^0, 90°, 180° and 270° with respect to the vertical axis. This whole antenna structure is fixed at the fuselage area in the aircraft. While interrogation occurs in Mode S and C, 1.03 GHz RF signal is transmitted by the antenna through the four monopole stubs. During the signal reception, all those radiating stubs detect the available 1.09 GHz RF signals. Phases of all the received signals are obtained from those directions of which the RF signals are received. Figure 3(b) shows the bottom mounted omnidirectional antenna, and it

Received 9 August 2017, Accepted 17 September 2017, Scheduled 27 September 2017
* Corresponding author: Debajit De (de.debajit118@ieee.org).
The authors are with the Department of Electrical Engineering, National Institute of Technology, Rourkela, India.

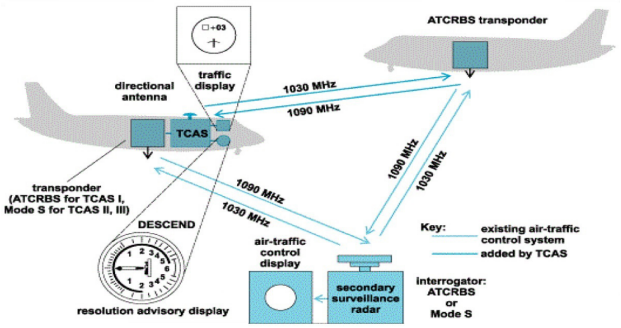

Figure 1. Mid air surveillance.

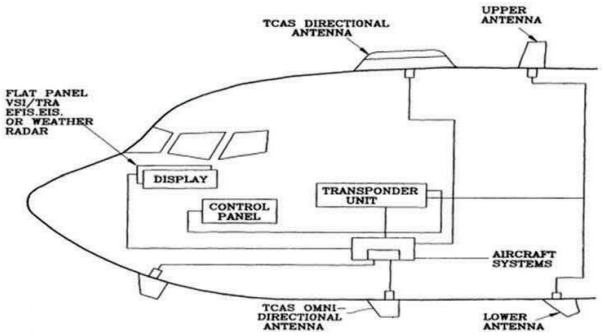

Figure 2. TCAS system block diagram.

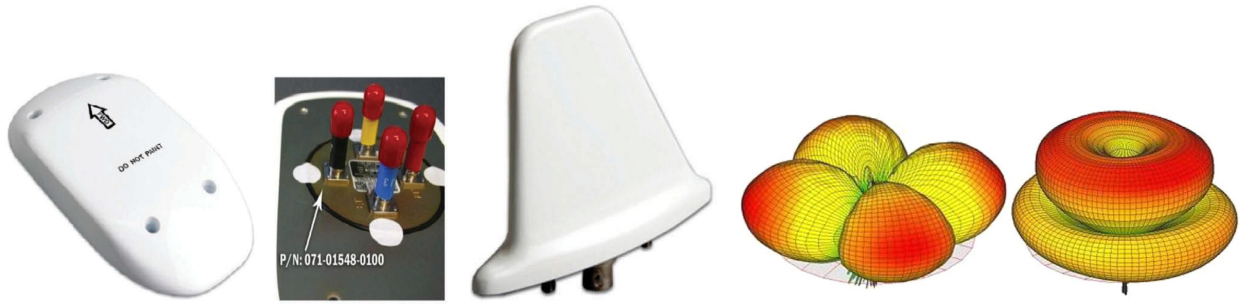

(a) (b) (c)

Figure 3. Existing TCAS antenna. (a) Directional, (b) omnidirectional and (c) it's radiation pattern.

is attached specifically at the underside of the aircraft to collect the range and altitude data of those traffics which are below the aircraft. This omnidirectional antenna has one L-band blade-shaped dipole component. The radiation pattern of four monopole stubs is shown in Figure 3(c). The four monopoles are mounted in such a pattern that the whole antenna structure can track all the surveillance area around the aircraft.

The antennas having end-fire radiation are widely preferable in many applications for their characteristics such as simplified structure, easy fabrication, cost effectiveness and low aerodynamic profile. Specially in airborne electronic system like TCAS, there is a restriction on the antenna orientation as it should not obstruct the airflow during flight. Hence, end-fire antenna is suitable for being used in these applications [4]. The radiation characteristics of the end-fire antenna depend on the antenna structure through which the surface wave propagates and its magnitude. These antennas are like Yagi antenna [5], helix antenna with end-fire mode [6], and tapered slot antenna [7]. Today, Microstrip Antennas have found wide application in the wireless communication field because of their attractive features such as low weight, low profile, small size and easy manufacture. It is a fact that microstrip antennas have intrinsically narrow bandwidth [8]. Much research has been done to increase their bandwidth, such as employing a multi-layer structure with aperture coupling [9] and adding parasitic elements [10]. However, in many practical cases, microstrip antennas are required not only to be wideband but also to have an end-fire radiation pattern. However, most previous researches of microstrip antennas mainly paid attention to the impedance bandwidth of antennas but ignored the radiation pattern to a certain extent. Very few attempts were made to achieve an end-fire radiation pattern from microstrip antenna.

This paper focuses on designing a microstrip antenna with end-fire radiation for a TCAS system of civil aircraft. The basic property of microstrip antenna is to radiate in the broadside direction. In this work, an attempt has been made to establish the concept that a microstrip antenna with simple modified configuration can also radiate in the end-fire direction just as those other conventional end-fired antennas. Again, microstrip antennas are well suited for this application because of their

narrow bandwidth characteristics. Moreover, frequency tuning, radiation beam shaping, tuning and steering/scanning are possible in microstrip antennas [11–14]. Microstrip antennas are very much mechanically robust which is one of the significant advantages for using them in this application [15].

Section 2 of this paper explains the design methodology of the proposed multi-feed microstrip antenna and its aerodynamically shaped radome. Section 3 deals with the simulation and measurement results of that proposed model. The discussions and summary of these results are also included in this section. The conclusion of this paper is provided in Section 4.

2. ANTENNA CONFIGURATION AND DESIGN ASPECTS

Figure 4(a) shows the proposed antenna, which is designed and simulated in CST Microwave Studio. Here, Chemical Etching process is used to fabricate the antenna. The fabricated antenna model is shown in Figure 5(a). FR4 Epoxy is chosen as the substrate material whose dielectric constant (ε_r) is 4.4, and thickness is 4 mm. Though FR4 Epoxy is a lossy material, it is used here, because this material is easily available in the market and very much cost effective. 1.06 GHz is chosen as the design frequency, since it is the center frequency between 1.03 GHz and 1.09 GHz. The dimensions of this proposed antenna are calculated using the formulas available in the literature [16].

An aerodynamically shaped radome is also designed here. It is made of PTFE coated fabric material. The proposed antenna is enclosed inside that radome, as shown in Figure 4(b) and Figure 5(b). The back side of that antenna with radome is shown in Figure 5(c). Four small metallic strips are used as the clips for tight and compact fixing of the antenna inside the radome. As the radome will be directly in contact with the air, it is designed with a proper aerodynamic shape [17]. Hence, the proposed radome will have minimum airflow resistance to the aircraft.

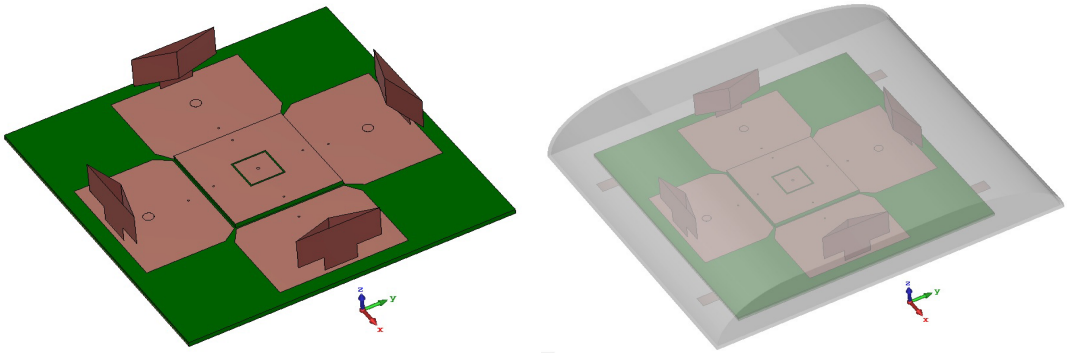

(a) (b)

Figure 4. Proposed antenna. (a) Simulated model and (b) simulated model inside a radome.

(a) (b) (c)

Figure 5. (a) Fabricated antenna model, (b) fabricated radome and (c) bottom view of the antenna model with radome.

This proposed antenna consists of total five patches out of which the center patch is treated as the common radiator, and the remaining four patches behave as the primary radiators. Before designing this antenna, a Dual Patch Dual Feed Microstrip Slotted Antenna was proposed [18]. That paper shows how end-fire radiation can be achieved using microstrip radiators for TCAS application. However, in that case, the antenna element only radiates in 0° direction of the azimuth plane. Hence, in this paper, that antenna structure is modified and implemented in such a way so that its radiation can cover the whole 360° region of the azimuth plane.

To steer the beam in all directions, 4 separate elements of Dual Patch Dual Feed Microstrip Slotted Antenna can be oriented at 0°, 90°, 180° and 270°. But in that case, the overall structure will be quite large, and it will not be compact. So, to make it compact and precise, this antenna structure is proposed. Now, if the whole antenna is assumed to be a cavity, then the cavity size should remain the same in all aspects so that it can resonate at its proper frequencies. However, in this proposed case, the antenna size is reduced which causes the size reduction of the cavity in terms of length and width. So, to make a proper cavity size, the thickness of the structure is increased. Hence, an additional 4 mm layer of FR4 substrate is added above the main substrate and under the center patch. Thus, the total height of the substrate area under the center patch becomes 8 mm, while the substrate height in the rest of the antenna remains 4 mm.

In this antenna structure, total five Shorting Pins/Inductive Posts are used, and they are drilled inside the substrate under all the five patches separately. The center patch also has one square-shaped ring type slot. Since the center patch is responsible for 1.03 GHz while patches 1, 2, 3 and 4 are responsible for 1.09 GHz, the design aspect behind the slot and shorting pin is to tune the frequencies 1.03 GHz and 1.09 GHz, respectively. Shorting pin provides inductance, and slot with length less than $\lambda_0/4$ provides capacitance to the overall antenna. As the frequency goes high, inductive reactance dominates, and as the frequency goes low, capacitive reactance dominates. So, by tuning the diameter of the shorting pin and length of the slots, a proper resonating frequency is achieved here. In this case, the shorting pins and slot can be treated as the tuning parameters.

Figure 6(a) shows a triangle-shaped metallic cap made of thin copper foil, which was proposed in the case of dual-patch dual-feed microstrip slotted antenna, and how it played a major role for obtaining the end-fire radiation and to reduce the back lobe was shown [18]. The height of that metallic cap was 65 mm in that design. Here in this proposed antenna, the height of the metallic cap is made considerably lower (40 mm) through the use of top-loaded elements [2] as shown in Figure 6(b). This modification considerably improves the air drag performance of the antenna structure.

The dimensions of this proposed antenna are provided in Table 1.

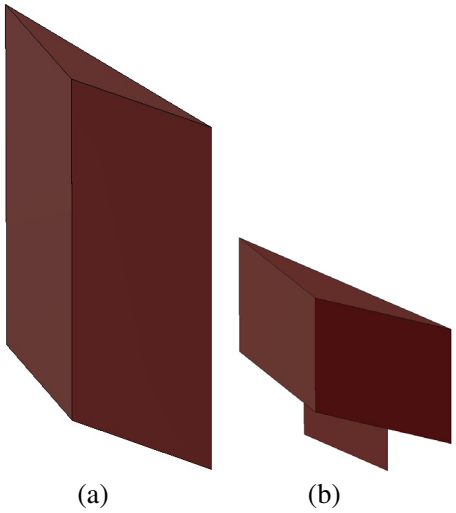

Figure 6. Triangular shaped metallic cap. (a) Normal structure and (b) top-loaded structure.

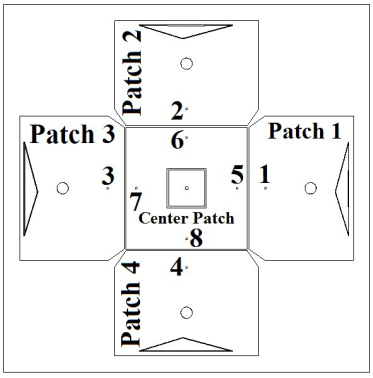

Figure 7. Patch and port numbering of the proposed antenna.

Table 1. Dimensions of the proposed antenna and it's radome.

Section	Dimension (In millimeter)
Substrate (Length × Width × Height)	224 × 224 × 4
Center Patch (Length × Width)	74 × 74
Patch 1, 2, 3 and 4 (Length × Width)	88 × 64
Square Ring Slot (Length × Width × Thickness)	18 × 18 × 2
Diameter of the Shorting Pin under Center Patch	3
Diameter of the Shorting Pin under Patch 1–4	7
Gap between Center Patch and other Patches	2
Height of the Top-Loaded Metallic Cap	40
Radome (Length × Width × Height)	304 × 264 × 45

Table 2. Direction of the antenna radiation beam with its corresponding ports excitation.

Case Number	Ports Excitation	Ports Matched Terminated	Direction of Radiation Beam
1	1 and 5	2, 3, 4, 6, 7 and 8	$+0^\circ$
2	1, 5, 2 and 6	3, 4, 7 and 8	$+45^\circ$
3	2 and 6	1, 3, 4, 5, 7 and 8	$+90^\circ$
4	2, 6, 3 and 7	1, 4, 5 and 8	$+135^\circ$
5	3 and 7	1, 2, 4, 5, 6 and 8	$+180^\circ$ or -180°
6	3, 7, 4 and 8	1, 2, 5 and 6	-135°
7	4 and 8	1, 2, 3, 5, 6 and 7	-90°
8	4, 8, 1 and 5	2, 3, 6 and 7	-45°

Here, to excite all these 5 radiating patches individually, total eight coaxial feeds are used in this proposed antenna. An equal split 1 : 8 RF Power Divider (ZN8PD-272SMP+ manufactured by Mini-Circuits) is utilized to feed this multi-port antenna. In this power divider, there is no phase difference among all the 8 output ports. The numbering of patches and ports in this antenna is very much essential, which is illustrated in Figure 7. By exciting proper port combinations, the antenna radiation beam can be continuously steered in the horizontal plane with 45° step in rotation. Hence, to steer the whole 360° region, total eight combinations for ports excitation are sufficient. In each combination, some antenna ports will be excited, and all the remaining ports will be terminated by 50 Ω matched terminator. Table 2 shows the details of it.

3. RESULTS AND DISCUSSIONS

The proposed antenna is simulated, fabricated and tested for the validation of the design technology. For the measurement and testing purpose, Agilent E5071C Vector Network Analyzer (VNA) is used. The radiation patterns of these proposed antennas are measured in a Tapered Anechoic Chamber with 10° step of rotation in the positioner. During the antenna gain measurement, a double-ridge horn antenna is used as the reference antenna.

The simulated and measured return losses of the proposed antenna are shown in Figure 8. From the simulated return loss plot of the antenna inside the radome, it is observed that S_{11}, S_{22}, S_{33} and S_{44} are around -55 dB at 1.03 GHz. Similarly, the simulated S_{55}, S_{66}, S_{77} and S_{88} are around -25 dB at 1.09 GHz. Again, from the measured return loss plot of the antenna inside the radome, it is shown that S_{11}, S_{22}, S_{33} and S_{44} are around -37 dB at 1.028 GHz. Similarly, the measured S_{55}, S_{66}, S_{77} and

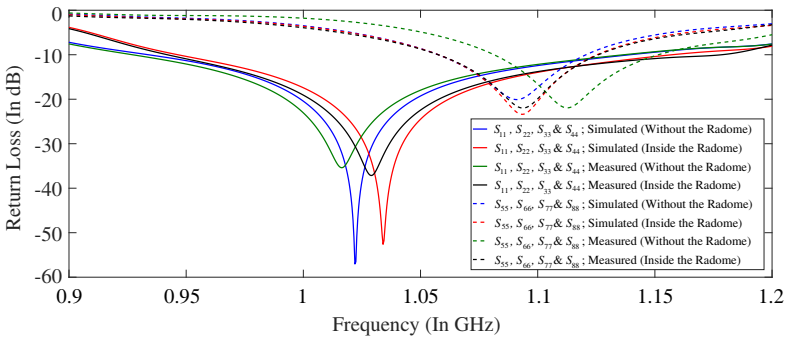

Figure 8. Simulated and measured return loss plot.

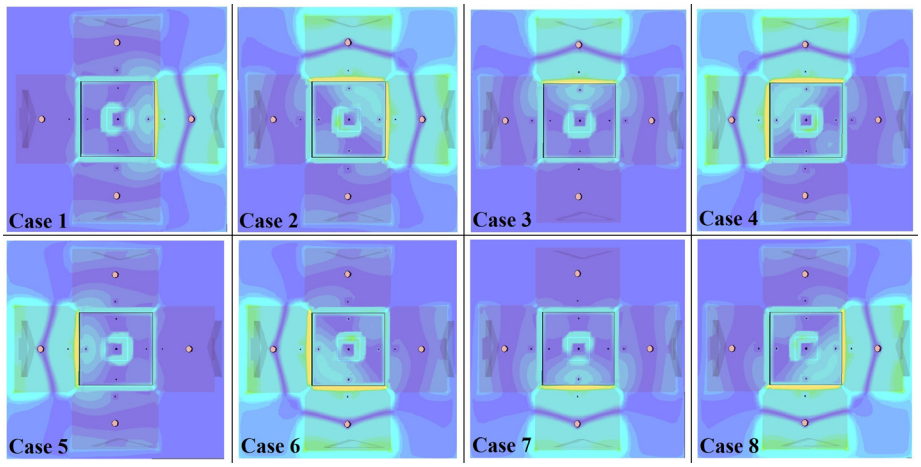

Figure 9. Simulated electric field distribution in the proposed antenna.

S_{88} are around -22 dB at 1.095 GHz. The simulated and measured return losses of the antenna without the radome are also illustrated in this plot. The measured return loss is in good agreement with the simulated ones, though there are a few disagreements due to measuring environment and fixation of the SMA connectors which are not taken care of during simulation.

Figure 9 and Figure 10 show the Electric Field Distribution and 3D Radiation Pattern of the proposed antenna, respectively. For both the operating frequencies of 1.03 GHz and 1.09 GHz, the simulated e-field distribution and 3D radiation pattern are almost similar. It is observed that the electric field is properly distributed in patch 1, patch 1 and patch 2, patch 2, patch 2 and patch 3, patch 3, patch 3 and patch 4, patch 4, patch 4 and patch 1 for case 1, case 2, case 3, case 4, case 5, case 6, case 7 and case 8, respectively. This also causes proper end-fire orientation of the radiation beam from the antenna in all these cases.

3.1. Power Patterns of the Proposed Antenna

In general, the whole body of the aircraft is itself a ground plane. Hence during the power pattern measurement, the proposed antenna is placed over a large metallic ground plane of size 10 m $\times$ 10 m for realizing the presence of the aircraft body up to some extent. It has been observed that the natures of antenna power patterns are almost similar for 1.03 GHz and 1.09 GHz. First, the antenna is tested without the radome, and then keeping the antenna inside the radome, it is tested again. All these scenarios are demonstrated below.

For case 1, the simulated and measured power patterns of the antenna inside the radome are shown in Figure 11(a). From this figure, it can be seen that the antenna radiates maximum at around $\varphi = 0^\circ$ of the XY azimuth plane for both the operating frequencies. Here, co-polarization level is

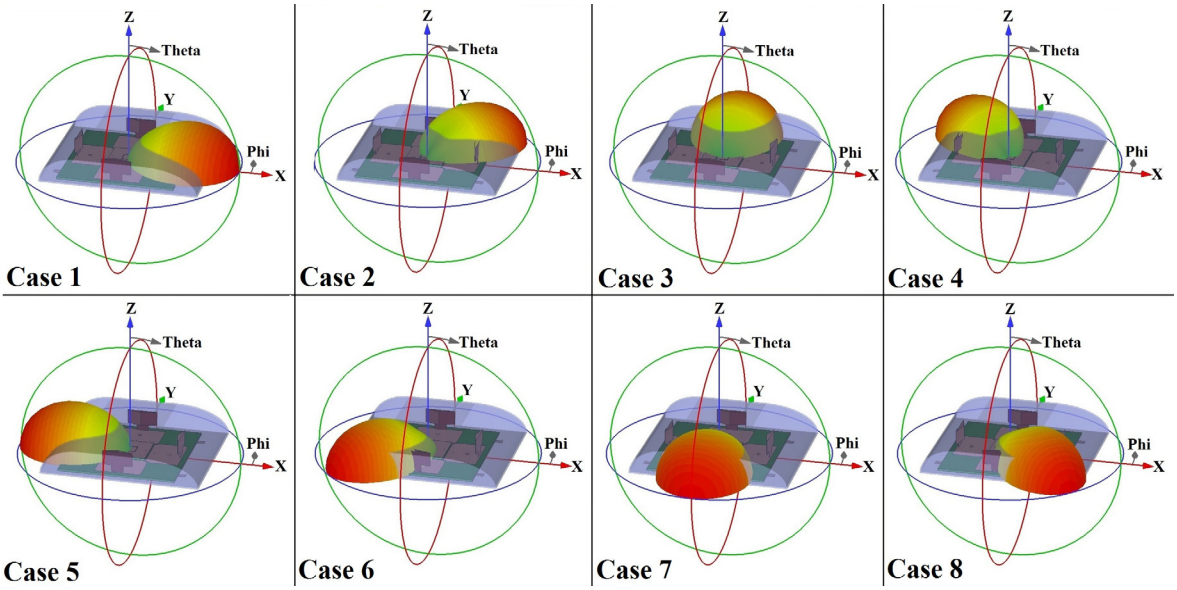

Figure 10. Simulated 3D radiation pattern of the proposed antenna.

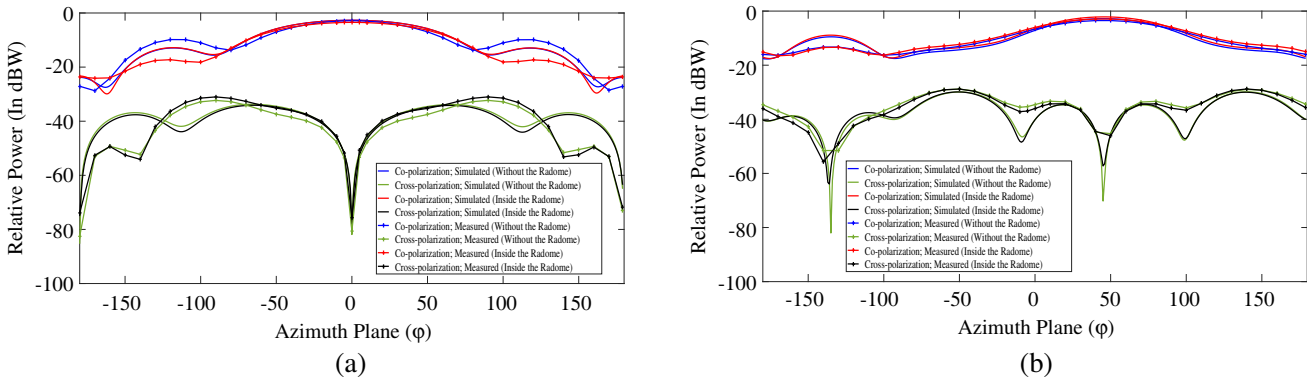

Figure 11. Simulated and measured power patterns plot for (a) case 1 and (b) case 2.

around −2.1 dBW, and the cross-polarization level is well below −40 dBW. Similarly, for case 2, the simulated and measured power patterns of the antenna are shown in Figure 11(b). From this figure, it is shown that the antenna radiates maximum at around $\varphi = +45°$ of the XY azimuth plane. Here, co-polarization level is around −2.4 dBW, and the cross-polarization level is well below −40 dBW. For both the cases, the co-pol is not affected by the cross-pol.

For case 3, the simulated and measured power patterns of the antenna are shown in Figure 12(a). From this figure, it can be seen that the antenna radiates maximum at around $\varphi = +90°$ of the XY azimuth plane. Similarly, for case 4, the simulated and measured power patterns of the antenna are shown in Figure 12(b). From this figure, it is shown that the antenna radiates maximum at around $\varphi = +135°$ of the XY azimuth plane.

For case 5, the simulated and measured power patterns of the antenna are shown in Figure 13(a). From this figure, it can be seen that the antenna radiates maximum at around $\varphi = +180°$ or $\varphi = -180°$ of the XY azimuth plane. Similarly, for case 6, the simulated and measured power patterns of the antenna are shown in Figure 13(b). From this figure, it is shown that the antenna radiates maximum at around $\varphi = -135°$ of the XY azimuth plane.

For case 7, the simulated and measured power patterns of the antenna are shown in Figure 14(a). From this figure, it can be seen that the antenna radiates maximum at around $\varphi = -90°$ of the XY

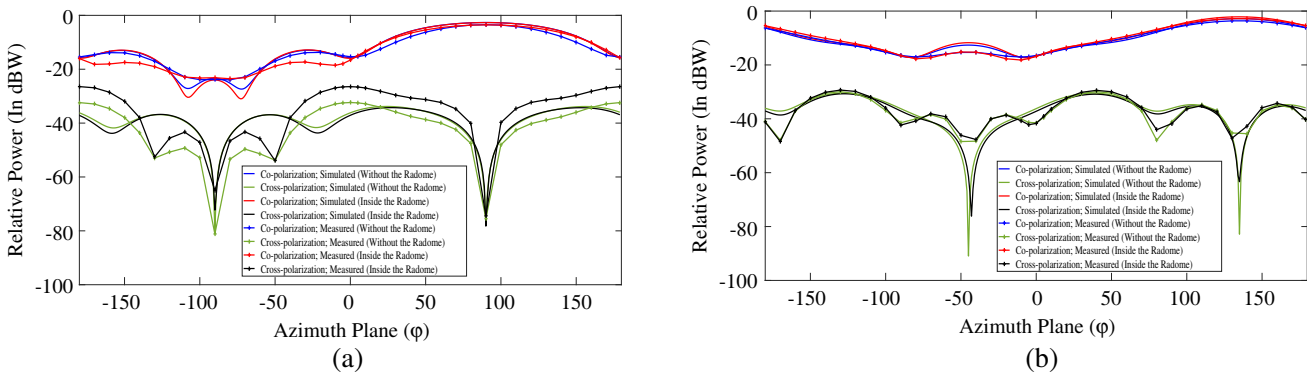

Figure 12. Simulated and measured power patterns plot for (a) case 3 and (b) case 4.

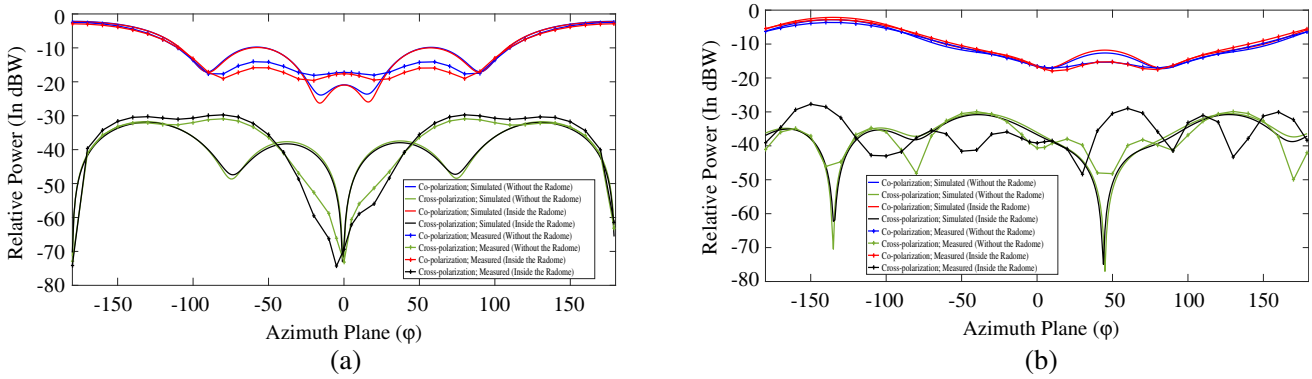

Figure 13. Simulated and measured power patterns plot for (a) case 5 and (b) case 6.

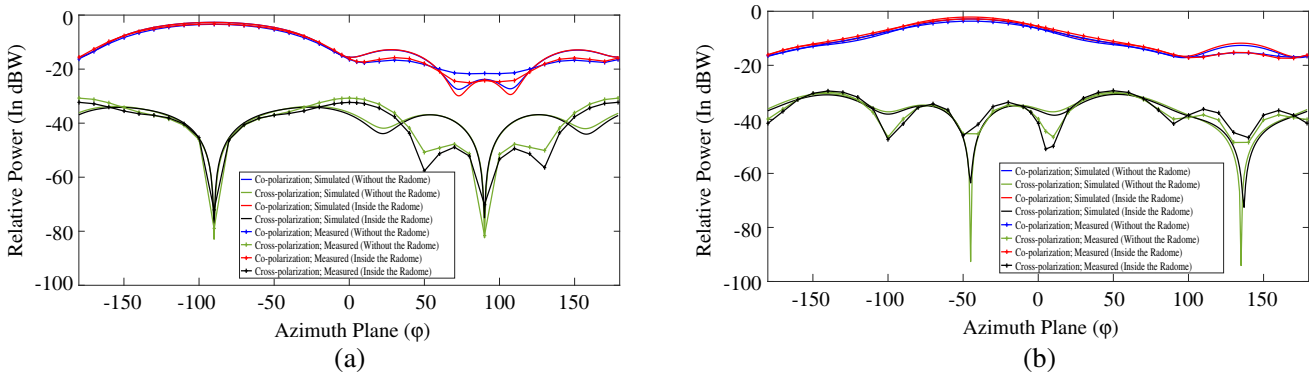

Figure 14. Simulated and measured power patterns plot for (a) case 7 and (b) case 8.

azimuth plane. Similarly, for case 8, the simulated and measured power patterns of the antenna are shown in Figure 14(b). From this figure, it is shown that the antenna radiates maximum at around $\varphi = -45^\circ$ of the XY azimuth plane.

3.2. Gain and Radiation Efficiency of the Proposed Antenna

The gain and radiation efficiency of the proposed antenna are measured without the radome and inside the radome. For all the cases, the simulated gain and radiation efficiency are shown below followed by the measured results.

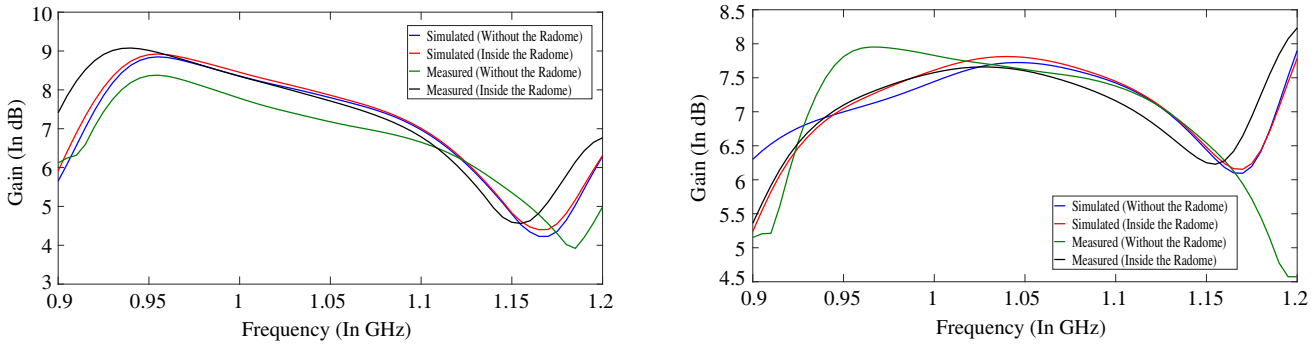

Figure 15. Simulated and measured antenna gain plot for (a) case 1, 3, 5, 7 and (b) case 2, 4, 6, 8.

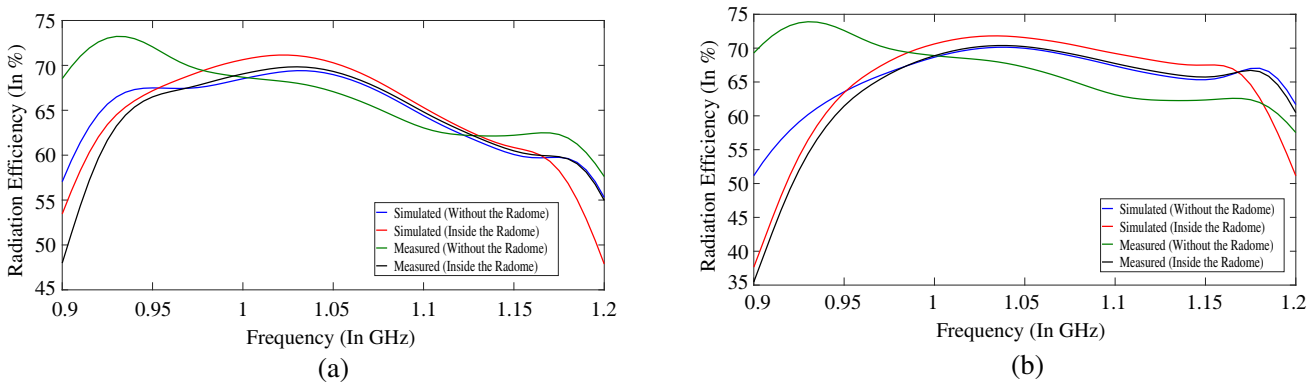

Figure 16. Simulated and measured antenna radiation efficiency plot for (a) case 1, 3, 5, 7 and (b) case 2, 4, 6, 8.

For cases 1, 3, 5 and 7, Figure 15(a) shows the simulated and measured peak gains of the proposed antenna inside the radome. It is observed that the simulated antenna gain is around 8.2 dB at 1.03 GHz and around 7.9 dB at 1.09 GHz. The measured antenna gain is around 8 dB at 1.028 GHz and around 7.7 dB at 1.095 GHz. Similarly, in Figure 15(b), the simulated and measured peak gains of the proposed antenna are shown for cases 2, 4, 6 and 8. Here, the simulated gain is around 7.8 dB at 1.03 GHz and around 7.4 dB at 1.09 GHz. The measured gain is around 7.5 dB at 1.028 GHz and around 7.1 dB at 1.095 GHz.

For cases 1, 3, 5 and 7, Figure 16(a) shows the simulated and measured radiation efficiencies of the proposed antenna inside the radome. It is observed that the simulated antenna radiation efficiency is around 70% at 1.03 GHz and around 67% at 1.09 GHz. The measured antenna radiation efficiency is around 68% at 1.028 GHz and around 65% at 1.095 GHz. Similarly, in Figure 16(b), the simulated and measured radiation efficiencies of the proposed antenna are shown for cases 2, 4, 6 and 8. Here, the simulated radiation efficiency is around 71% at 1.03 GHz and around 69% at 1.09 GHz. The measured radiation efficiency is around 69% at 1.028 GHz and around 66% dB at 1.095 GHz.

3.3. Air Drag Performance of the Proposed Antenna with the Radome

Airflow Resistance is one type of force which influences the objects that travel through the air. This is one of the important parameters to understand the motion of the fast moving objects such as aircraft. It depends on the air density, cross-sectional area of the object, moving velocity of the object and a drag coefficient which is due to other properties of the object, such as the surface roughness and turbulence. Airflow resistance is also called as Air Drag, and this force is generally measured in Newtons (N).

In this work, the standard equation [19] is used for measuring the force of air resistance on the

aircraft due to the proposed antenna. The standard drag coefficient is chosen as 0.024. By calculating, it is obtained that the cross-sectional area of the of the proposed antenna with radome is 0.08 m^2. The air density varies with the altitude and temperature. As the altitude from the sea level goes high, the air density is decreased. A commercial aircraft can maximum fly up to around 12 km from the sea level. As the aircraft climbs up at the higher altitudes, its speed is also increased. Generally, during take-off and landing, the speed of the commercial aircraft varies around 200–250 km/hr, and while traveling in mid-air, the maximum achievable speed at the highest altitude is around 900 km/hr.

Table 3 demonstrates the air drag performance of this proposed antenna. The air drag is calculated for various aircraft speeds at different altitudes. From this table, it can be seen that the air density is deceased with the increment of altitude from the sea level. These data of air density are collected from the US Standard Atmosphere Air Properties [20]. Here, it is also stated that when an average speed of the aircraft is around 548 km/h at the altitude of 6 km from the sea level, the air drag on the aircraft is 14.7 N for the proposed antenna. As the altitude of the aircraft from the sea level is increased, the aircraft's speed is also increased, which causes substantial increment in air drag values. Throughout the traveling of the aircraft from take-off to landing, the air drag performance of the existing TCAS antenna varies from 4 N to 21 N while in the case of this proposed antenna, it varies from 3.6 N to 20.8 N. Hence, the air drag performance of the proposed antenna is expected to be satisfactory.

Table 3. Calculated air drag of the proposed antenna with the radome.

Altitude from Sea Level (m)	Air Density (kg/m^3)	Speed of Aircraft (km./hr.)	Air Drag (N)
0	1.225	200	3.6
1000	1.112	258	5.5
2000	1.007	316	7.5
3000	0.909	374	9.4
4000	0.819	432	11.3
5000	0.736	490	13.1
6000	0.660	548	14.7
7000	0.590	606	16.0
8000	0.526	664	17.2
9000	0.467	722	18.0
10000	0.414	780	18.7
11000	0.380	838	19.8
12000	0.350	896	20.8

3.4. Performance Comparison between the Proposed and the Existing Monopole TCAS Antenna

Table 4 summarizes all the simulation and measurement results of the proposed antenna. This table also helps to observe the performance comparison between the proposed and the existing monopole TCAS antenna [21]. It is found that this 8-feed microstrip antenna provides better performance than the existing monopole TCAS antenna in terms of frequency sensitivity, desired end-fire radiation pattern, gain, beamwidth and side-lobe level. Hence, this prototype antenna model can be a better product for this application.

Comparing the S parameters as seen from the Table 4, it is clear that the frequency sensitivity is better for the proposed antenna. The VSWR values of the proposed antenna are well matched as that of existing antenna. It is seen that the gain of the proposed antenna is roughly doubled which implies

Table 4. Performance comparison between the proposed and the existing monopole TCAS antenna.

Parameters			**Proposed Antenna (Without Radome)**	**Proposed Antenna (With Radome)**	**Existing Monopole TCAS Antenna**
Operating Frequencies (In GHz)	f1	Simulated	1.022	1.03	1.03
		Measured	1.02	1.028	
	f2	Simulated	1.087	1.09	1.09
		Measured	1.11	1.095	
Return Loss (In dB)	at f1	Simulated	−58	−55	−15
		Measured	−35	−37	
	at f2	Simulated	−21	−25	
		Measured	−24	−22	
VSWR	at f1	Simulated	1.06	1.07	1 to 1.5
		Measured	1.10	1.11	
	at f2	Simulated	1.41	1.23	
		Measured	1.28	1.39	
Gain (In dB)	at f1	Simulated	8.1	8.2	3.5
		Measured	7.5	8	
	at f2	Simulated	7.9	7.9	
		Measured	7.0	7.7	
Beamwidth (In degree)	at f1	Simulated	54°	53°	More than 100°
		Measured	55°	54°	
	at f2	Simulated	55°	54°	
		Measured	56°	55°	
Side Lobe (In dB)	at f1	Simulated	−12.1	−12.4	−7.5
		Measured	−12.4	−12.6	
	at f2	Simulated	−11.9	−12.1	
		Measured	−12.0	−12.6	
Radiation Efficiency (In %)	at f1	Simulated	69	71	-
		Measured	66	69	
	at f2	Simulated	66	69	
		Measured	63	66	
Range of Air Drag (In Newton)			-	3.6 to 20.8	4 to 21

that the power expenditure during signal transmission is economized. From Table 4, it is also observed that the beamwidth of the proposed antenna is roughly reduced to half as compared to that of the existing TCAS antenna. Due to this narrow beamwidth, resolving the location of the intruder aircraft in terms of bearing angle is much better, and hence the resolution power of this proposed antenna is better than the existing one. The current TCAS antenna which is fitted in the aircraft has the side lobe level of −7.5 dB, as shown in Table 4, while the side lobe level of the proposed antenna is around −12 dB which is almost half of the said magnitude of the existing antenna. Hence, the sensitivity of the proposed antenna is expected to be better. Due to this low level of side lobe in the proposed antenna and if this low level is considered to be the threshold value of return signal, the covering distance will likely become more than the existing antenna. As the covering distance is larger, larger number of aircraft, which are unseen in the existing system, can be detected. So, larger number of aircraft can be tracked for collision probability with respect to its own aircraft.

4. CONCLUSION

This paper presents a designing technique for a microstrip antenna which can be used in TCAS application. The proposed prototype model of the antenna provides a better performance, such as high gain, good directivity and narrow beamwidth than that of existing monopole TCAS antennas. The whole antenna structure can radiate towards the 360° surveillance region around the aircraft with proper excitation of the corresponding ports. The ongoing research focus is on the development of a reconfigurable/switchable feeding network, and it will be designed in such a way that the input power will be fed to proper antenna ports with various switching conditions. Hence, the antenna beam can be steered in the whole azimuth plane by just controlling a few RF switches. The proposed antenna is very compact in size and weights around only 550 grams. This antenna is also cost effective since an FR4 epoxy substrate is used here. The width and length of the patch are determined for conforming to the space section accessible for the overall fuselage area in the aircraft. To encapsulate the antenna inside an enclosure, an aerodynamically shaped radome is proposed here. It is shown that the airflow resistance to the aircraft due to this radome is within the limit. Therefore, for a TCAS airborne system, the proposed multi-feed end-fired microstrip antenna would be expected to meet the requirements of the advanced avionics standards in terms of design simplicity, lightweight and high performance.

ACKNOWLEDGMENT

The authors would like to acknowledge the college authority of National Institute of Technology, Rourkela, India for various financial support during this research work.

REFERENCES

1. Henely, S., *The Avionics Hand Book, 18-TCAS II*, Rockwell Collins, Cedar Rapids, 2001.
2. Harman, W. H., "TCAS: A system for preventing midair collisions," *The Lincoln Laboratory Journal*, Vol. 2, 437–458, 1989.
3. Kuchar, J. K. and A. C. Drumm, "The traffic alert and collision avoidance system," *The Lincoln Laboratory Journal*, Vol. 16, 277–296, 2007.
4. Sanyal, J. A., A. Basu, S. K. Koul, M. Abegaonkar, S. Varughese, and P. B. Venkatesh Rao, "A planar end-fire array in S-band for airborne applications," *IETE Journal of Research*, Vol. 58, No. 1, 34–43, 2014.
5. De Jean, G. R., T. T. Thai, S. Nikolaou, and M. M. Tentzeris, "Design and analysis of microstrip Bi-Yagi and Quad-Yagi antenna arrays for WLAN applications," *IEEE Antennas and Wireless Propagation Letters*, Vol. 6, 244–248, 2007.
6. Ehrenspeck, H., "The double-helix antenna and its variants, a new class of tunable endfire antennas," *IEEE Transactions on Antennas and Propagation*, Vol. 13, No. 2, 203–208, 1965.
7. Pazin, L. and Y. Leviatan, "A compact 60-GHz tapered slot antenna printed on LCP substrate for WPAN applications," *IEEE Antennas and Wireless Propagation Letters*, Vol. 9, 272–275, 2010.
8. Kraus, J. D. and R. J. Marhefka, *Antennas: For All Applications*, 3rd Edition, The McGraw-Hill Companies Inc., 2002.
9. Targonski, S. D., R. B. Waterhouse, and D. M. Pozar, "Design of wide-band aperture-stacked patch microstrip antennas," *IEEE Transactions on Antennas and Propagation*, Vol. 46, No. 9, 1245–1251, 1998.
10. Abdelaziz, A., "Bandwidth enhancement of microstrip antenna," *Progress In Electromagnetics Research*, Vol. 63, 311–317, 2006.
11. Saed, M. A., "Broadband CPW-fed planar slot antennas with various tuning stubs," *Progress In Electromagnetics Research*, Vol. 66, 199–212, 2006.
12. Kale, G. M., R. P. Labade, and R. S. Pawase, "Tunable and dual band rectangular microstrip antenna for bluetooth and WiMAX applications," *Microwave and Optical Technology Letters*, Vol. 57, No. 8, 1986–1991, 2015.

13. Attia, H., O. Siddiqui, and O. Ramahi, "Beam tilting of single microstrip antenna using high permittivity superstrate," *Microwave and Optical Technology Letters*, Vol. 55, No. 7, 1657–1661, 2013.
14. Wu, W., B. Z. Wang, and S. Sun, "Pattern reconfigurable microstrip patch antenna," *Journal of Electromagnetic Waves and Applications*, Vol. 19, No. 1, 107–113, 2012.
15. Orban, D. and G. J. K. Moernaut, "The basics of patch antennas," *RF Globalnet Newsletter*, 2009.
16. Balanies, C. A., *Antenna Theory: Analysis & Design*, 2nd Edition, John Wiley & Sons Inc., 1997.
17. *Installation Manual Bendix/King KR 87 Automatic Direction Finder, Manual Number 006-00184-0006*, Honeywell, 2006.
18. De, D. and P. K. Sahu, "An investigation on end-fire radiation from linearly polarized microstrip antenna for airborne systems," *Progress In Electromagnetics Research M*, Vol. 59, 9–24, 2017.
19. *Air Resistance Formula*, www.softschools.com/formulas/physics/air_resistance_formula/85/, 2005.
20. *U.S standard atmosphere, NOAA-S/T76-1562*, National Oceanic and Amospheric Administration, National Aeronautics and Space Administration and United States Air Force, 1976.
21. *TCAS S72-1735-25, AIRNC 735*, Sensor Systems Inc., Aircraft Antennas since 1961.